Chinese Journal of
POLYMER SCIENCE

RESEARCH ARTICLE

https://doi.org/10.1007/s10118-022-2813-2
Chinese J. Polym. Sci. **2023**, *41*, 267–277

Multifunctional Waterborne Polyurethane Nanocomposite Films with Remarkable Electromagnetic Interference Shielding, Electrothermal and Solarthermal Performances

Ming-Ke Xu[a,b], Xin-Jie Luo[a], Hao-Bin Zhang[a*], Yu Zhang[b], Lu-Lu Li[a], Xin-Feng Zhou[b], and Zhong-Zhen Yu[b*]

[a] *Beijing Key Laboratory of Advanced Functional Polymer Composites, Beijing University of Chemical Technology, Beijing 100029, China*
[b] *State Key Laboratory of Organic-Inorganic Composites, College of Materials Science and Engineering, Beijing University of Chemical Technology, Beijing 100029, China*

Electronic Supplementary Information

Abstract To impart polymers with high electrical conductivity and satisfactory electromagnetic interference shielding efficiency, it is crucial to efficiently construct interconnecting networks of conductive nanofillers in polymer matrices. Herein, on the basis of the three-dimensional (3D) skeleton and volume-exclusion effect of silane-modified tetra-needle ZnO (ST-ZnO) whiskers and the high conductivity of two-dimensional MXene nanosheets, multifunctional MXene/ST-ZnO/waterborne polyurethane (MTW) nanocomposite films are fabricated by coating of MXene on ST-ZnO followed by compounding with waterborne polyurethane. The 3D four-needles of the whiskers facilitate the formation of an interconnecting network in the waterborne polyurethane matrix, while the coating of MXene efficiently makes the interconnecting network of the whiskers conductive at a low amount of the MXene. The resultant MTW ternary nanocomposite film exhibits not only a high electrical conductivity of 4.8×10^4 S/m, but also an excellent electromagnetic interference shielding effectiveness of over 70 dB in the X-band at a low thickness of 100 μm. In addition, the ternary film also exhibits outstanding Joule heating performances with an equilibrium temperature of 113 °C at a low driving voltage of 3 V. The multifunctional nanocomposite films are promising for applications in portable and wearable electronics and flexible electromagnetic interference shielding devices.

Keywords Electrical conductivity; Electromagnetic interference shielding; Nanocomposite films; Waterborne polyurethane; MXene nanosheets

Citation: Xu, M. K.; Luo, X. J.; Zhang, H. B.; Zhang, Y.; Li, L. L.; Zhou, X. F.; Yu, Z. Z. Multifunctional waterborne polyurethane nanocomposite films with remarkable electromagnetic interference shielding, electrothermal and solarthermal performances. *Chinese J. Polym. Sci.* **2023**, *41*, 267–277.

INTRODUCTION

With the rapid development of communication technology and the integration of electronic equipment, electromagnetic wave radiation and interference become increasingly serious, which not only interferes with the normal operation of nearby high-precision instruments, but also poses a great threat to human health.[1–4] It is therefore imperative to develop high-performance electromagnetic interference (EMI) shielding nanomaterials and nanocomposites to diminish or eliminate the electromagnetic wave pollution.[5] Electrically conductive polymer composites are widely used for EMI shielding applications because of their light weight, superb corrosion resistance, outstanding processability, and tunable properties.[6–8] Furthermore, the rapid popularity of portable and wearable electronic devices increases the demands for polymer nanocomposite films with high shielding efficiency and small thickness for EMI shielding applications.[9–11] To construct effective interconnecting networks of conductive nanofillers in polymer matrices, conductive nanofillers with both high aspect ratio and large specific surface area are preferred, such as graphene nanosheets,[12–14] carbon nanotubes (CNTs)[15–17] and MXene nanosheets.[10,18,19] Different from hydrophobic graphene and CNTs with inert surfaces, MXene is hydrophilic because of its rich surface chemistry, which would facilitate its dispersion in polar polymers without additional surface treatments. However, if conductive nanofillers are dispersed randomly in polymer matrices, satisfactory EMI shielding performances of polymer nanocomposites were usually achieved at higher contents of nanofillers and/or larger thicknesses,[20,21] which adversely affects the flexibility of the EMI shielding nanocomposites and even causes processing difficulties.[22]

Both the dispersion and distribution of conducting nanofillers in polymer matrices are crucial for achieving high electrical conductivities and satisfactory EMI shielding performances at low contents of nanofillers.[23] When the conducting

* Corresponding authors, E-mail: zhanghaobin@mail.buct.edu.cn (H.B.Z.)
E-mail: yuzz@mail.buct.edu.cn (Z.Z.Y.)

Received May 7, 2022; Accepted June 10, 2022; Published online September 26, 2022

nanofillers are selectively dispersed in the continuous phase of a polymer blend, or distributed only at the interfaces of the two polymer components, the percolation thresholds of conductive polymer nanocomposites can be decreased significantly.[24,25] In addition, the combination of different types of fillers is also effective in promoting the formation of interconnecting networks in polymers for improving electrical conductivity, thermal conductivity, and mechanical performances.[26–30] For example, Wu *et al.*[31] constructed a carbon black-based three-dimensional (3D) conductive structure in natural rubber matrix with cellulose whiskers as templates, enhancing the electrical and mechanical properties of the natural rubber nanocomposites. Similarly, Xu *et al.*[9] designed 3D conductive fillers based on tetra-needle zinc oxide (T-ZnO) whiskers and Ag nanoparticles for fabricating conductive waterborne polyurethane (WPU) nanocomposite films with outstanding EMI shielding performances. Despite these advances, it is still desirable to achieve a higher EMI shielding effectiveness at a smaller film thickness.[32]

Compared with conventional organic polymers, WPU is environmentally friendly as its dispersion medium is water instead of organic solvents, and has excellent film-formability and outstanding flexibility.[33] It is well suitable for preparing flexible functional films.[15,34] To impart flexible WPU films with high electrical conductivity, satisfactory EMI shielding effectiveness (SE), Joule heating behavior, and solar-thermal conversion performances, we fabricate WPU-based nanocomposite films by coating silane-modified tetra-needle ZnO (ST-ZnO) whiskers with conductive MXene nanosheets followed by compounding with WPU. The unique four-needles of the whiskers can be readily interconnected to generate a continuous network in the WPU matrix. Although the whiskers are not electrically conductive, the coating of MXene on the ST-ZnO whiskers can efficiently make the interconnecting network of the whiskers conductive at a low amount of MXene. Obviously, the whiskers play the role of hosting the conducting MXene nanosheets, and exhibit a volume-exclusion effect on promoting the spatial distribution and interconnection of conducting nanofillers and hence the formation of an electrical conduction network. As a result, the resultant MXene/ST-ZnO/WPU (MTW) nanocomposite films exhibit higher electrical conductivities and better EMI shielding performances than those of MXene/WPU (MW) binary nanocomposite films with the same MXene contents. Notably, the MTW ternary nanocomposite film with a small thickness of 100 μm achieves a high EMI SE of over 70 dB in the X-band. Additionally, the ternary films exhibit satisfactory Joule heating and solar-thermal conversion performances at low-voltage driving or under solar-light irradiation, which are promising for warming and heating electronic devices properly to avoid malfunctions of the devices in cold environments.[35,36]

EXPERIMENTAL

Materials

Tetra-needle ZnO (T-ZnO) whiskers were obtained from Chengdu Crystrealm Co., Ltd. (China). Waterborne polyurethane emulsion (Crysol 6110) with a solid content of 50 wt% was provided by Wanhua Chemicals (China). Silane coupling agent of (3-aminopropyl) triethoxysilane (APTES) was bought from Shanghai Yuanye Biotechnology (China). Ti_3AlC_2 (400 mesh) and Lithium fluoride (LiF, 99.99%) powders were supplied by Jilin 11 technology and Aladdin (China), respectively. Hydrochloric acid (HCl, 37%) was acquired from Beijing Chemical Reagents (China).

Preparation of $Ti_3C_2T_x$ MXene Nanosheets

Ti_3AlC_2 powder was etched with HCl/LiF solution as previously reported.[37,38] In detail, 8 g of LiF powder was dissolved in 100 mL of HCl solution (9 mol/L) under stirring, and 5 g of Ti_3AlC_2 powder was then added slowly and carefully. After the mixture reacted for 42 h in a water bath at 35 °C with magnetic stirring, the resultant acidic suspension was repeatedly washed with plenty of deionized water with the assistance of centrifugal separation until its pH value was ~6. Finally, the centrifuged sediment was re-dispersed in deionized water and ultrasonicated in an ice bath for 1 h under the protection of argon flow to obtain exfoliated $Ti_3C_2T_x$ MXene nanosheets.

Fabrication of Silane-modified T-ZnO Whiskers

The surface of T-ZnO whiskers was modified with the silane coupling agent to introduce amine groups. Typically, 200 mg of T-ZnO whiskers were dispersed in 200 mL of the solution of absolute alcohol and deionized water (1/1, *V*/*V*), and sonicated for 5 min. After 1 mL of APTES was added, the mixture reacted at 50 °C for 4 h under magnetic stirring, centrifuged at 9500 r/min for 15 min, and washed with absolute alcohol for 3 times to remove residual APTES. The product was dried in an oven at 80 °C for 3 h, and designated as ST-ZnO.

Fabrication of Conductive MXene/ST-ZnO/WPU and MXene/WPU Nanocomposite films

Firstly, the ST-ZnO whiskers and the MXene dispersion were mixed in a 50 mL centrifugal tube by a vortex machine at 1000 r/min for 5 min, and the mixture was then mixed with the WPU emulsion under ultrasonication for 10 min. Subsequently, the MXene/ST-ZnO/WPU mixture was casted into a culture dish to form a film, dried at 50 °C for 24 h, and peeled from the culture dish. The MXene/ST-ZnO/WPU (MTW) ternary nanocomposite films with different MXene contents and thicknesses were prepared by varying the dosages of ST-ZnO, MXene and WPU, and keeping the MXene/ST-ZnO mass ratio of 2:1. The MTW nanocomposite films with 0.5 wt%, 1 wt%, 2 wt%, 5 wt%, 10 wt%, 20 wt%, 30 wt%, 40 wt% and 50 wt% of MXene were designated as MTW0.5, MTW1, MTW2, MTW5, MTW10, MTW20, MTW30, MTW40 and MTW50, respectively. Similarly, the MTW ternary films with a constant content of MXene (10 wt%) but different MXene/ST-ZnO mass ratios (1/1 and 3/1) were also prepared, and designated as a-MTW10 and c-MTW10, respectively. For comparison, MXene/WPU (MW) binary nanocomposite films with 0.5 wt%, 1 wt%, 2 wt%, 5 wt%, 10 wt%, 20 wt%, 30 wt% and 50 wt% of MXene were prepared by direct mixing of MXene and WPU followed by casting, and designated as MW0.5, MW1, MW2, MW5, MW10, MW20, MW30 and MW50, respectively. In the absence of the MXene, the binary ST-ZnO/WPU film (TW15) was also prepared by compounding 15 wt% of ST-ZnO with WPU.

Characterizations

Microstructures were observed with a Hitachi 7700

https://doi.org/10.1007/s10118-022-2813-2

transmission electron microscope (TEM), and a Hitachi S4700 scanning electron microscope (SEM). X-ray diffraction (XRD) patterns were recorded using a Rigaku D/Max 2500 X-ray diffractometer. The chemical compositions were analyzed by a Thermo VG RSCAKAB 250X X-ray photoelectron spectroscopy (XPS), and a Nicolet 8700 Fourier-transform infrared (FTIR) spectrometer. Zeta potentials were measured by a Malvern Nano-ZS Zetasizer. Electrical conductivities were evaluated with a Keithley 6517B resistivity meter and a 4-probes Tech RST-8 resistivity meter. The EMI shielding performances were measured on a Keysight N5224B PNA series vector network analyzer within the frequency range of 8.2–12.4 GHz. A UTM4502XH universal tensile tester was used to measure tensile properties of the films at a speed of 5 mm/min. Infrared thermal images were recoded with a FLIR-E40 thermal imager.

RESULTS AND DISCUSSION

Microstructures of the MXene/ST-ZnO Nanofillers

Fig. 1(a) illustrates the fabrication process of multifunctional MTW ternary films. First, to enhance the interfacial interaction between MXene nanosheets and the T-ZnO whiskers, the whiskers are modified by the silane coupling agent to introduce active amine groups. Because of the interaction of the positively charged ST-ZnO (12.8 mV) with the negatively charged MXene nanosheets (−44 mV), the surface of ST-ZnO can be wrapped by polar MXene nanosheets to form MXene/ST-ZnO hybrid nanofillers. Subsequently, the hybrid nanofillers are compounded with WPU, and the mixture is casted and dried to generate multifunctional MTW ternary films, which are expected to exhibit excellent EMI shielding efficiency, and satisfactory Joule heating and solar-thermal conversion performances for wearable electronics served in cold environments (Fig. 1b).

$Ti_3C_2T_x$ MXene nanosheets are obtained by selective etching of the Ti_3AlC_2 MAX phase with the HCl/LiF solution followed by ultrasonic exfoliation.[39] As confirmed by the XRD patterns, the successful removal of the Al layer is reflected by the weakening or almost disappearance of some peaks of the Ti_3AlC_2, including (101), (103), (104), (105), (107), (108), and (109) lattice planes (Fig. S1a in the electronic supplementary information, ESI). After the etching, the (002) diffraction peak of the MXene shifts from 9.5° to 7.1°, indicating enlarged intra-galleries due to the intercalation of lithium ions and water molecules.[40] After the ultrasonic exfoliation, the (002) diffraction peak shifts further to 6.8°, and the remaining characteristic peaks of the Ti_3AlC_2 disappears, confirming the formation of ultrathin $Ti_3C_2T_x$ MXene nanosheets (Figs. S1b and S1c in ESI).[6]

To enhance the adhesion of the MXene nanosheets with T-ZnO, the surface of the T-ZnO is modified by the silane coupling agent of APTES to generate active amine groups. The MXene nanosheets can be coated on the surface of the modified whiskers (ST-ZnO) by the attractive positive and negative charges.[27,41,42] The modification of T-ZnO can be verified by the XPS and FT-IR spectra of ST-ZnO (Figs. S2a and S2b in ESI). Compared with the T-ZnO, the ST-ZnO present two additional peaks at 399.6 and 102.0 eV, corresponding to N 1s and Si 2p, respectively. Moreover, the FTIR spectrum of the ST-ZnO shows representative absorbance bands of stretching vibrations of —OH and Zn—O at 3442 and 507 cm^{-1}, respectively (Fig. S2b in ESI). The characteristic absorption band of Zn—O—Si bond appears at 1093 cm^{-1}, and the typical bands at 2926 and 2854 cm^{-1} can be attributed to the asymmetric and symmetric stretching vibrations of $—CH_2$ of APTES.[43,44] In addition, the ST-ZnO exhibits the same typical diffraction peaks as the T-ZnO at 31.9°, 34.6°, 36.4°, 47.6°, and 56.7°, corresponding to the (100), (002), (101), (102), and (110) lattice planes, respectively, which is consistent with the hexagonal wurtzite structure of ZnO (JCPDS36-1451),[27,41,45] implying that the crystal structure of T-ZnO is not affected by the silane modification.[46]

The influences of the MXene/ST-ZnO mass ratio (1/0, 1/1, 2/1 and 3/1) on the electrical conductivity and EMI shielding performance of their WPU nanocomposite films (MW10, a-MTW10, MTW10, and c-MTW10) are compared (Fig. S3 in ESI). Clearly, the MTW10 film containing the hybrid nanofillers with

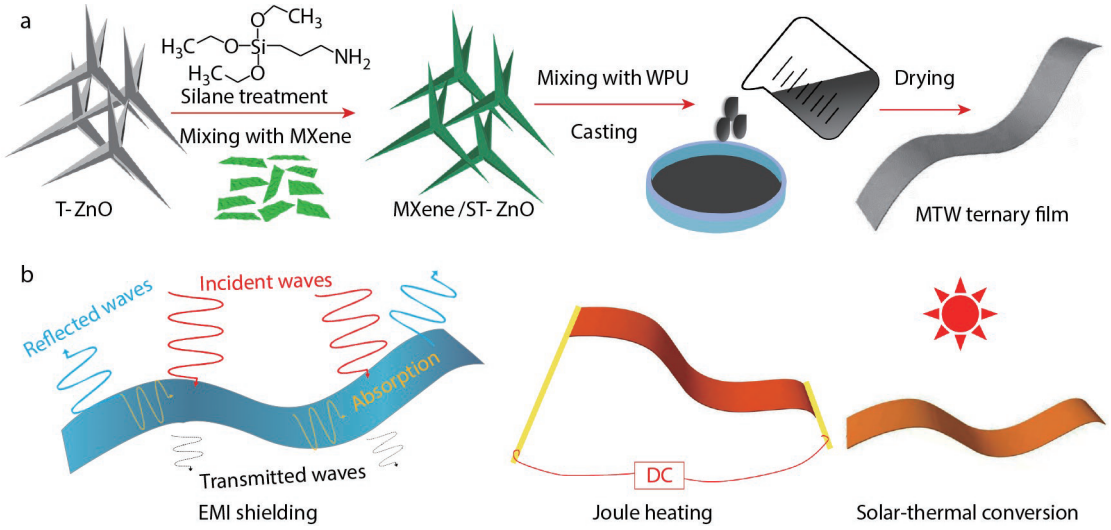

Fig. 1 (a) Schematic illustrating the fabrication of a MXene/ST-ZnO/WPU (MTW) nanocomposite film and (b) its multifunctional applications.

an MXene/ST-ZnO mass ratio of 2/1 exhibits the highest electrical conductivity and average EMI shielding efficiency in the X-band. Therefore, the MXene/ST-ZnO nanofillers with a mass ratio of 2/1 are chosen for fabricating the ternary nanocomposite films unless otherwise specified.

The coating of MXene on the ST-ZnO whiskers is crucial for constructing efficient conduction networks in WPU matrix. The chemical compositions of MXene, and the MXene/ST-ZnO hybrid nanofillers are identified by their XPS spectra (Fig. 2a). The Ti 2p XPS spectrum of MXene presents distinct C-Ti-T_x $2p_{3/2}$ (455.4 eV) and C-Ti-T_x $2p_{1/2}$ (461.5 eV) peaks, and abundant surface functional groups (—OH, —F, and —O), endowing the MXene with strong electronegativity and good dispersability in water (Figs. S4a and S4b in ESI). The introduced amine groups on the ST-ZnO are also verified by the two strong fitting peaks at ~399.4 eV for C—NH_2 and 400.7 eV for protonated —N^+H_3 in the N 1s XPS spectrum of ST-ZnO (Fig. 2b).[47] However, in the N 1s spectrum of the MXene/ST-ZnO nanofillers, both the peaks of C—NH_2 and protonated —N^+H_3 shift to higher binding energies and a new peak of Ti-N bonding at ~396.8 eV appears (Fig. 2c), which should derive from the interfacial interaction between the unstable titanium terminations of MXene and the amine groups of the ST-ZnO.[42] The enhanced interaction between the MXene and the modified whiskers would facilitate the coating of the whiskers with the MXene. The presence of the strong peaks of C-Ti-T_x $2p_{3/2}$ (455.4 eV) and C-Ti-T_x $2p_{1/2}$ (461.5 eV) in the Ti 2p XPS spectrum of MXene/ST-ZnO (Fig. 2d) further confirms the coating of MXene on the whiskers.[6,18]

Furthermore, the successful coating of MXene nanosheets on the surfaces of ST-ZnO can be confirmed by SEM images of ST-ZnO, and MXene/ST-ZnO hybrid nanofillers (Figs. 2e and 2f). Clearly, ST-ZnO shows a tetrapod stereo structure with a smooth surface (Fig. 2e). As expected, the MXene/ST-ZnO exhibits a similar tetrapod stereo conformation, but has a rough surface because of the coated MXene sheets (Fig. 2f). The conductive coating makes the whiskers conductive, which is highly efficient in constructing an interconnecting conduction network at a much lower MXene content.[9,46]

Microstructures, Electrical Conductivities and EMI Shielding Performances of MTW Ternary Films

To confirm the advantage of the unique 3D structure of the MXene/ST-ZnO, Figs. 3(a) and 3(b) compare the electrical conductivities of the MTW ternary nanocomposite films with those of the MW binary nanocomposite films. Pure WPU film is typically insulating with a low conductivity of 2.8×10^{-12} S/m. Although the electrical conductivities of both the ternary and binary films improve with increasing the MXene content, the MTW ternary films exhibit higher electrical conductivities than those of the MW binary films at the same MXene contents. Moreover, the MTW ternary films present a faster transition from electrically insulating to conducting at a much lower MXene content than those of the MW binary films (Fig. 3a).[48] For example, although the electrical conductivities of MTW0.5 and MW0.5 films are 4.0×10^{-9} and 9.4×10^{-10} S/m, respectively, when the MXene content increases to 1.0 wt%, MTW1 film exhibits a rapidly increased electrical conductivity of 4.3×10^{-3} S/m, nearly 6 orders of magnitude higher than that of the MW1 film. In addition, as the MXene content increases from 20 wt% to 50 wt%, the electrical conductivity of the MTW ternary film improves further from 1.3×10^{3} S/m to 4.8×10^{4} S/m, while the conductivity of the MW binary film increases only from 5.4×10^{2} S/m to 2.0×10^{4} S/m (Fig. 3b). The better electrical performances of the MTW ternary films can be attributed to the volume-exclusion effect of the ST-ZnO skeleton, leading to an increase in the effective concentration of MXene in the WPU matrix.[49] The unique 3D structure of the ST-ZnO whiskers facilitates their interconnection to form a conductive network at a smaller MXene content.[50–52] Similarly, at a given MXene content, the MTW ternary films exhibit better EMI shielding performances in the X-band than those of their binary counterparts (Fig. 3c).

In addition, the electrical conductivities and EMI shielding

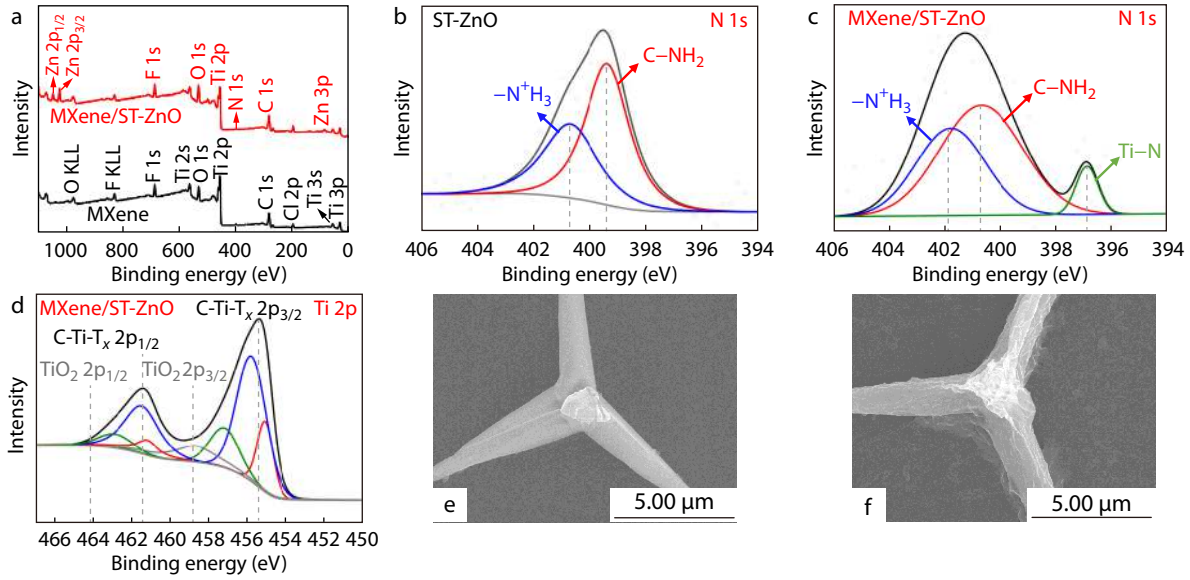

Fig. 2 (a) XPS survey spectra of MXene, and MXene/ST-ZnO. N 1s XPS spectra of (b) ST-ZnO, and (c) MXene/ST-ZnO. (d) Ti 2p XPS spectrum of MXene/ST-ZnO. SEM images of (e) ST-ZnO, and (f) MXene/ST-ZnO.

https://doi.org/10.1007/s10118-022-2813-2

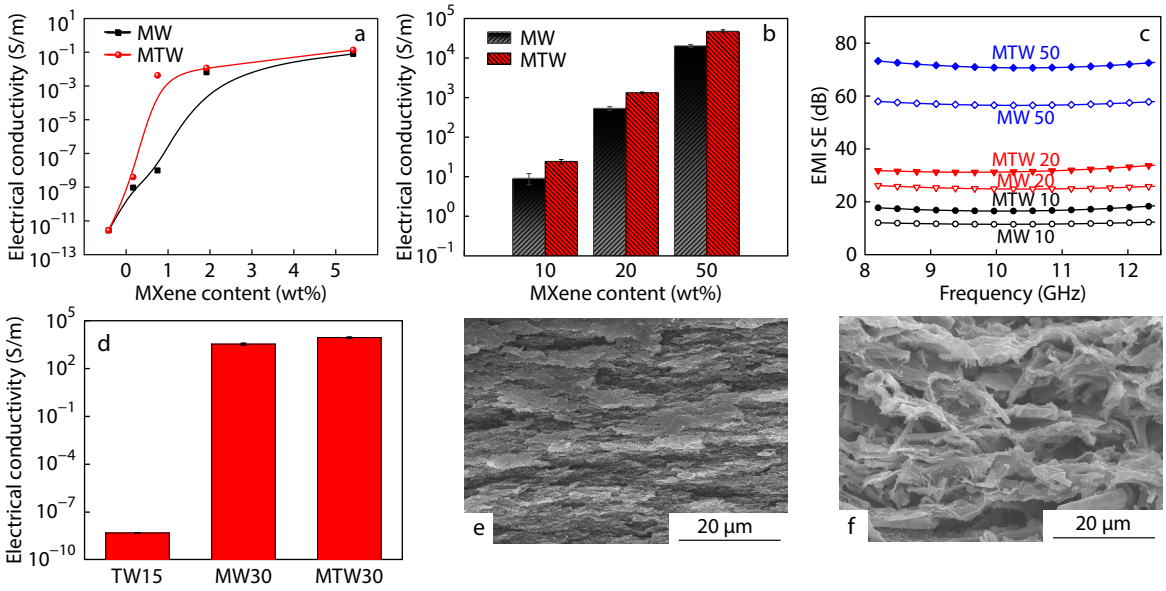

Fig. 3 (a) Plots of electrical conductivity versus MXene content for MTW and MW films; (b) Electrical conductivities, and (c) EMI shielding performances of the MTW and MW films; (d) Comparison of electrical conductivities of different nanocomposite films; Cross-sectional SEM images of (e) MW30 film, and (f) MTW30 film.

properties of MTW30, MW30, and TW15 films are compared to highlight the advantages of the MTW ternary films (Fig. 3d, Fig. S5 in ESI). The electrical conductivities of MTW30, MW30, and TW15 films are 8.7×10^{3}, 3.4×10^{3} and 4.7×10^{-9} S/m, respectively (Fig. 3d). Reasonably, the TW15 film has a low electrical conductivity of 4.7×10^{-9} S/m, only slightly higher than that of pure WPU film, indicating that 15 wt% of ST-ZnO alone has a negligible improvement in the conductivity of WPU. Consistent with the electrical properties, the MTW30 film shows better EMI shielding performances compared to the MW30 film and the TW15 film (Fig. S5 in ESI). As a comparison, the TW15 film exhibits poor average EMI SE (~0.2 dB) in the X-band due to its low electrical conductivity. On the other hand, the fractured surfaces of MW30 film and MTW30 film are observed to ascertain the dispersion states of the fillers, thereby analyzing the reasons for the different electrical conductivities of various films (Figs. 3e and 3f, Fig. S6 in ESI). Compared with the MTW30 film, MXene nanosheets in the MW30 film are randomly distributed in WPU matrix (Fig. 3e and Fig. S6a in ESI), which is responsible for its lower electrical conductivity and poorer EMI shielding performance. As mentioned above, the surfaces of ST-ZnO are readily coated with MXene nanosheets to form MXene/ST-ZnO hybrid nanofillers with typical "core-shell" structure (Fig. 2f). Importantly, when the MXene/ST-ZnO hybrid nanofillers are dispersed in WPU matrix, most of MXene nanosheets are still tightly attached to the surfaces of ST-ZnO and remain connected, thus forming continuous and dense conductive networks in the matrix (Fig. 3f and Fig. S6b in ESI).[50] Therefore, for the MTW30 film, based on the volume-exclusion effect of ST-ZnO with a unique 3D skeleton, the MXene nanosheets are interconnected to form a conductive network, resulting in higher electrical conductivity and better EMI shielding performance compared with MW30 binary films.[52,53]

Constructing continuous and highly efficient conductive networks in the WPU matrix through MXene/ST-ZnO hybrid nanofillers with special 3D structures is crucial for obtaining highly conductive MTW ternary films. Fig. 4(a) depicts the electrical conductivity of MTW ternary films with various MXene contents. Clearly, the electrical conductivity of the MTW ternary films rises rapidly with increasing MXene content. For instance, the electrical conductivity increases swiftly from 2.5×10^{1} S/m for the MTW10 to 8.7×10^{3} S/m for the MTW30 film, and further rises to 2.5×10^{4} S/m when the MXene content increases to 40 wt% (MTW40). Finally, the conductivity of the MTW50 film is as high as 4.8×10^{4} S/m. The superb electrical conductivities endow MTW ternary films with excellent EMI shielding performances.[54] As shown in Fig. 4(b), the EMI SE increases with the rising of MXene content, consistent with the variation tendency of electrical conductivity. Compared to pure WPU film (~0 dB), the MTW20 film with a thickness of 0.1 mm exhibits an average EMI SE of 31.8 dB in the X-band, which exceeds the minimum requirement of 20 dB for commercial applications.[18] With the further increase of MXene content, the EMI SE of the MTW50 film in the X-band exceeds 70 dB (0.1 mm), which can block 99.99999% of incident electromagnetic waves to meet the strict requirements of some military and civilian applications.[6,33,37,55] Furthermore, when the content of MXene increases from 10 wt% to 50 wt%, the contribution from absorption (SE_A) to the total attenuation of incident electromagnetic waves (SE_{Total}) at 12 GHz increases rapidly from 9.9 dB to 52.7 dB, while the contribution from reflection (SE_R) just rises from 7.8 dB to 19.2 dB (Fig. 4c), indicating the existence of an absorption-dominated EMI shielding mechanism in MTW ternary films.[33] The strengthened conductance network with increment of MXene content enhances the conduction loss of the MTW ternary films. Besides, massive interfaces extend the transmission path of the electromagnetic waves inside the nanocomposite films, resulting in great in-

https://doi.org/10.1007/s10118-022-2813-2

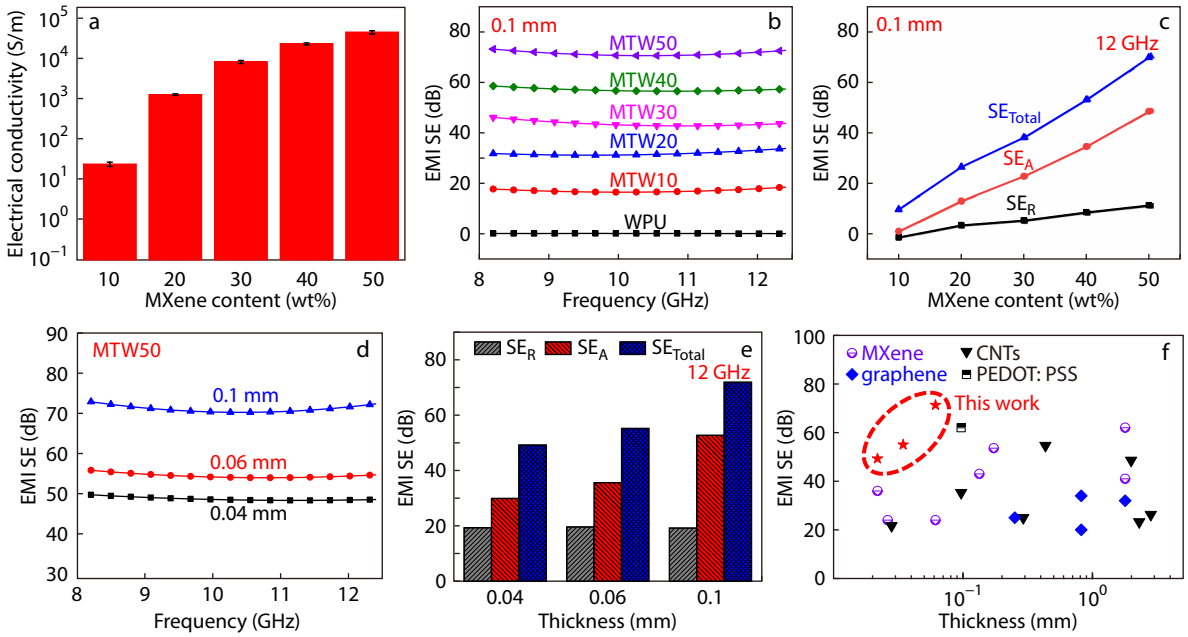

Fig. 4 Influences of MXene content on (a) electrical conductivity and (b) EMI SE of MTW ternary films in the X-band; (c) Effects of MXene content on SE_{Total}, SE_A, and SE_R of MTW ternary films at the frequency of 12 GHz; (d) Effect of sample thickness on EMI shielding effectiveness of MTW50 films; (e) Effects of sample thickness on SE_{Total}, SE_A, and SE_R of MTW50 films at the frequency of 12 GHz; (f) Comparison of EMI shielding performances of the MTW ternary films and those reported in the literature.

terfacial polarization and current accumulation for efficient absorption dissipation of electromagnetic waves. Moreover, the surface terminations, defects and heterogeneous interfaces could also enhance the electromagnetic wave dissipation by providing versatile dipole polarizations, leading to improved SE_A and SE_{Total}.[6,20,54]

In addition, the EMI shielding performances of the MTW50 films with various thicknesses are compared. Clearly, as the thickness increases from 0.04 mm to 0.06 mm and 0.1 mm, the average EMI SE in X-band improves from 49.4 dB to 55.1 dB and 71.4 dB, respectively (Fig. 4d). Moreover, as depicted in Fig. 4(e), the increased thickness leads to a large rise in SE_{Total} and SE_A, but the SE_R is almost unchanged, thus still exhibiting an absorption-dominated EMI shielding mechanism in the MTW ternary films. The EMI shielding advantage of the prepared MTW ternary films is further highlighted by comparing with other polymer-based EMI shielding materials reported (Fig. 4f, Table S1 in ESI). Recently, more and more researchers focus on conductive polymer composites to achieve outstanding EMI shielding properties.[2,56] However, in view of the low conductivity of polymer composites, large sample thicknesses are generally required to reach satisfactory EMI SE, such as the annealed $Ti_3C_2T_x$/epoxy nanocomposite (41 dB) with a thickness of 2 mm[20] and the CNT/polypropylene composite (48.3 dB) with a thickness of 2.2 mm.[25] This inevitably results in poor flexibility, thereby limiting the application of shielding materials. Alternatively, graphene, CNT, or MXene-based polymer nanocomposite films are reported for thin and flexible EMI shielding materials, whereas, their EMI shielding performances are generally non-ideal due to the large contact resistance. For instance, the EMI SE of the MXene/cellulose nanofiber composite paper with a thickness of 0.047 mm is 24 dB,[10] and the EMI SE of the CNT/NR composite film with a thickness of 0.05 mm is 21.4 dB.[16] Compared with the above results, MTW50 film exhibits a higher EMI SE of 49.4 dB at a thinner thickness of 0.04 mm, and has a ultrahigh normalized EMI SE/thickness of 1235 dB/mm, which is among the best performances of polymer-based EMI shielding materials (Fig. 4f, Table S1 in ESI).[6,15,57,58]

Considering that good mechanical properties are an important prerequisite for the application of electromagnetic shielding materials in practical environment,[22,59] the mechanical properties of MTW nanocomposite films, pure WPU film and pure MXene film are further tested. Fig. 5(a) shows the tensile stress-strain curves of MTW ternary films with various MXene contents, where the inset shows the digital photograph of MTW50 film in the bending state. Fig. 5(b) shows the corresponding tensile strength and elongation at break of MTW ternary films with various MXene contents. Obviously, the tensile strength of the MTW ternary films improves gradually as the MXene content increases from 20 wt% to 50 wt%, while their elongation at break decreases. In addition, Table S2 (in ESI) details the respective tensile strength and elongation at break of MTW10 film, MTW20 film, MTW30 film, MTW40 film, MTW50 film, pure WPU film, and pure MXene film. The tensile strength of pure WPU film is only 8.2 MPa, while that of MTW10 film increases to 16.2 MPa. When MXene content increases to 30 wt%, the tensile strength of MTW30 film further increases to 29.8 MPa. As the MXene content further increases to 50 wt%, the tensile strength of the prepared MTW50 film can reach 39.6 MPa, which is 383% higher than that of the pure WPU film, and much higher than that of the pure MXene film (22.2 MPa). It should be pointed out that, although the elongation at break of the prepared MTW ternary

https://doi.org/10.1007/s10118-022-2813-2

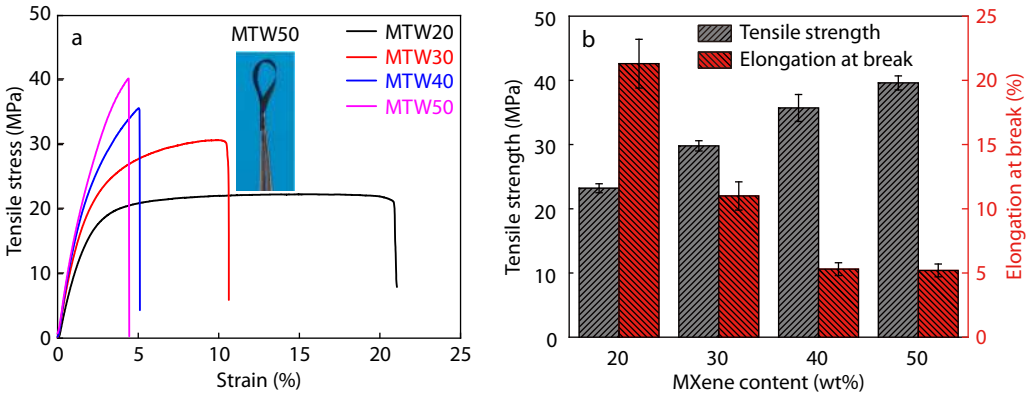

Fig. 5 (a) Typical tensile stress-strain curves of MTW ternary films with various MXene contents. The inset shows the digital photograph of MTW50 film under bending state. (b) Comparison of tensile strength and elongation at break of MTW ternary films with various MXene contents.

films decreases gradually with increasing MXene content, the MTW50 film still retains the ideal elongation at break of 5.2%, while the elongation at break of the pure MXene film is only 0.7% at the same tensile rate of 5 mm/min. In addition, the inset in Fig. 5(a) shows that the MTW50 film with a thickness of 0.1 mm still has good flexibility. On the other hand, the above conductivities and EMI shielding performances test results show that the conductivity of MTW50 film is as high as 4.8×10^4 S/m, and the average EMI SE in X-band reaches 71.4 dB at a thickness of 0.1 mm (Fig. 4b). Therefore, the MTW ternary films not only have excellent conductive and electromagnetic shielding performances, but also have satisfactory mechanical properties.

Joule Heating Performances of MTW Ternary Films

In addition to excellent EMI shielding properties, the MTW ternary films also exhibit outstanding Joule heating performances. Fig. 6 presents the Joule heating performances of MTW20 film (10 mm × 20 mm) at low driving voltages ranging from 1 V to 3 V. The almost linear *I-V* curve in Fig. 6(a) indicates that the film has a low and steady resistance (~14.5 Ω), which ensures the safety of low driving voltage heating to the human body, and allows the film to achieve outstanding Joule heating performances.[39,60,61] Moreover, it can be seen from the inset of Fig. 6(a) that the MTW20 film can be used as a wire in the circuit to light up a blue LED bulb, suggesting the good electrical conductivity of the film. Fig. 6(b) compares the Joule heating performances of MTW20 films at various driving voltages. Clearly, the equilibrium temperature of the film rises rapidly with increasing driving voltage, indicating the controllability and safety of Joule heating performances. For example, the film can reach an equilibrium temperature of ~51 °C at a lower driving voltage of 1.5 V, which further rises to ~92 and 113 °C at 2.5 and 3 V, respectively. In particular, at the driving voltage of 3 V, the film can attain a high temperature of ~78 °C within only 5 s, showing a rapid thermal response and efficient electrothermal conversion.[23,60] It is worth noting that, the equilibrium temperature of the film exhibits a superb linear relationship with the square of the driving voltage (Fig. 6c), which is consistent with the theoretical predictions for Joule heaters reported in previous researches.[22,61] Furthermore, as depicted in Fig. 6(d), the surface temperature of the film can be easily and rapidly adjusted by switching the driving voltage between 1 and 3 V.

Moreover, in order to evaluate the heating stability of the films, the temperature-time variation curve with a constant driving voltage of 3 V is investigated. As can be seen from Fig. 6(e), the surface temperature of the film is rapidly elevated to the equilibrium temperature, and shows only slight fluctuations during the long duration of ~1200 s, demonstrating the satisfactory long-term heating stability of the film. In addition, the heating/cooling cycles are performed on the film at a driving voltage of 3 V to assess the cyclic stability of the film heater (Fig. 6f). Clearly, the temperature evolution curves for the 1st, 5th and 10th cycles are almost overlapped, demonstrating the stability of the film during cyclic heating. To sum up, the MTW20 film demonstrates a satisfactory long-term heating reliability and wide temperature tunability at moderate and safe driving voltages, as well as rapid thermal response, which is superior to most film-based heaters reported in the literature (Table S3 in ESI).[60,62] The outstanding Joule heating performances of the film may be ascribed to its high electrical conductivity and low resistance.[22,42,61]

Furthermore, in order to explore the potential application of the MTW ternary film heater for de-icing or even heating water in outdoor icy weather, we connect the film (10 mm × 20 mm) to an external UTP1306S DC power supply by pieces of copper foil and crocodile clips, and then place a glass bottle with ice on the surface of the film to fabricate a simple deicing device. As shown in Figs. 6(g) and 6(h), after applying a constant voltage (3 V), the ice cube (~2.7 cm^3) in the glass bottle starts to melt rapidly, and can be completely melted within 840 s, while the temperature of the water increases from the original −0.3 °C to 20.9 °C. Moreover, the water can be further heated to a high temperature of 50.7 °C with the water vapor generated inside the glass bottle (Fig. 6h). In contrast, the temperature of the unheated ice cube increases slightly within 840 s (Fig. S7 in ESI).

Solarthermal Conversion Performances of MTW Ternary Films

It should be noted that the heating method utilizing the Joule heating effect requires a wired power supply, thus limiting the application scenarios of MTW ternary films.[63] Interestingly, in addition to the excellent EMI shielding properties and outstanding Joule heating performances, the MTW ternary films

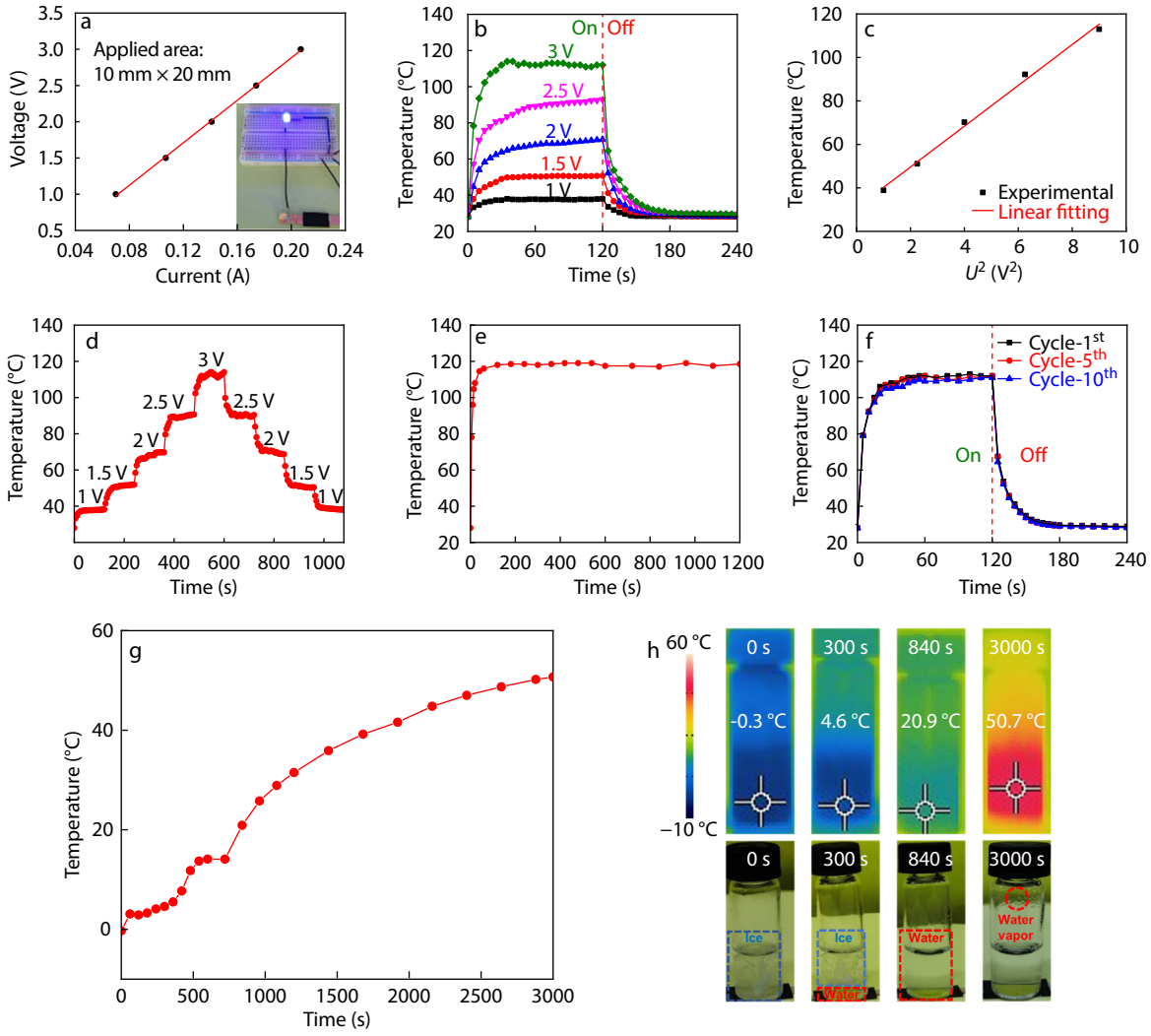

Fig. 6 (a) *I-V* curve and (b) Joule heating performances of MTW20 film; (c) Experimental data and linear fitting of equilibrium temperature versus U^2; (d) Temperature evolution curve under stepwise increased/decreased voltages for MTW20 film; (e) Temperature-stability and (f) cyclic Joule heating performance at a constant voltage of 3 V for MTW20 film; (g) Temperature evolution curve of the bottom ice/water with increasing time during the deicing process at a driving voltage of 3 V; (h) IR and digital images of the bottom ice/water at different time during the deicing process.

also exhibit decent solar-thermal conversion performances, which may be attributed to the localized surface plasmon resonance (LSPR) effect of MXene nanosheets.[64–66] It can be seen from Fig. 7(a) that the surface temperature of pure WPU film only slightly increases from room temperature (27 °C) to ~40 °C after 30 min of light irradiation with an intensity of 100 mW/cm^2 (one-sun irradiation). In contrast, the MTW20 film can quickly reach a high surface temperature around 63 °C and keep almost unchanged for a long time, indicating the superb and stable solar-thermal conversion performances of the MTW20 film.

Furthermore, Fig. 7(b) exhibits the temperature change curves of the MTW20 film under different illumination intensities for 90 s. Clearly, with the increase of illumination intensity, the MTW 20 film can obtain a higher surface temperature within the same irradiation time. Impressively, even under extremely low illumination intensity of 50 mW/cm^2, the MTW20 film can still reach a satisfactory surface temperature of around 40 °C within 90 s. Besides, a cyclic test (100 mW/cm^2) with an illumination period of 90 s is performed to assess the cycling stability of the MTW20 film (Fig. 7c). It should be pointed out that, the temperature change curves of the 1st, 15th, and 30th cycles are almost overlapped, demonstrating the very steady solar-thermal conversion performances of the film for periodic practical application.[35] Surprisingly, the MTW20 film still shows decent solar-thermal conversion performances even in a very cold environment. Fig. 7(d) schematically illustrates the experimental setup where the MTW20 film is irradiated by sunlight above liquid nitrogen to simulate a very cold environment (below −30 °C). Obviously, the surface temperature of the film drops dramatically with the decrease of the ambient temperature, making the originally flexible film gradually become brittle (Fig. 7e). As expected, when the film is irradiated at an illumination intensity of 100 mW/cm^2 for 800 s, its surface temperature can reach a satisfactory temperature of 20 °C with a temperature

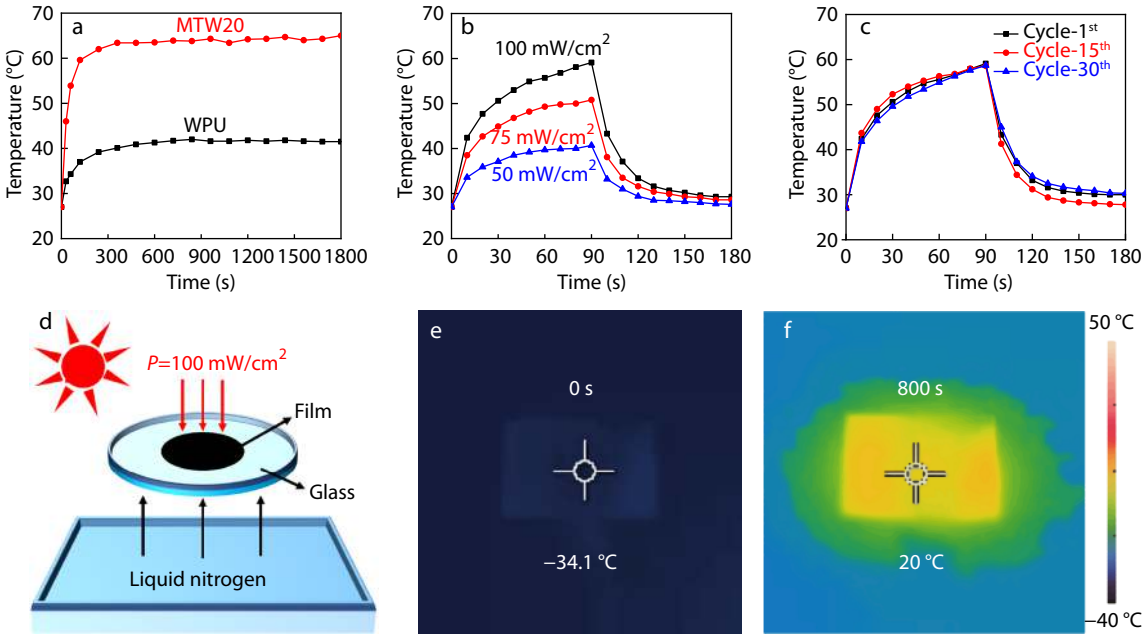

Fig. 7 (a) The temperature variation curves of pure WPU film and MTW20 film under the light irradiation of 100 mW/cm^2 for 30 min; (b) Temperature-time curves of the MTW20 film under different light irradiation intensities; (c) Cyclic solar-thermal performance of the MTW20 film under the light irradiation of 100 mW/cm^2; (d) Schematic simulated solar-thermal response of MTW20 film in a cold environment; IR images of MTW20 film placed on the cold glass culture dish (e) without light irradiation and (f) under light irradiation of 100 mW/cm^2.

increment of 50 °C, while the ambient temperature remains very low (Fig. 7f). The decent solar-thermal conversion performances of the MTW20 film ensure its self-heated ability by light irradiation, thereby avoiding the deterioration of flexibility and EMI shielding performance in extremely cold environment.[36] To sum up, MTW ternary films demonstrate decent Joule heating and solar-thermal conversion performances, which ensures their normal application in cold environments and expands their potential applicability.

CONCLUSIONS

Multifunctional MTW ternary films with high electrical conductivities, satisfactory EMI shielding performances, and excellent electrothermal and solar-thermal conversion properties are prepared by mixing MXene/ST-ZnO hybrids with WPU emulsion followed by casting and drying. Based on the unique 3D framework and volume-exclusion effect of ST-ZnO, MXene nanosheets can form a continuous and dense conductive network in the WPU matrix, which plays a crucial role in enhancing the electrical conductivities and EMI shielding performances of WPU nanocomposite films. Therefore, the resultant MTW ternary nanocomposite films exhibit higher electrical conductivities and EMI shielding performances than those of their MW binary counterparts with the same MXene mass contents and at similar sample thicknesses. Moreover, the MTW ternary film with a thickness of only 100 μm demonstrates a high EMI SE of over 70 dB in the X-band. The MTW ternary films also exhibit outstanding Joule heating performances with an equilibrium temperature of 113 °C at a low driving voltage of 3 V. The multifunctional MTW ternary films have broad application prospects in wearable electronics and EMI shielding devices served in extremely cold environments.

NOTES

The authors declare no competing financial interest.

Electronic Supplementary Information

Electronic supplementary information (ESI) is available free of charge in the online version of this article at http://doi.org/10.1007/s10118-022-2813-2.

ACKNOWLEDGMENTS

This work was financially supported by the National Natural Science Foundation of China (Nos. 51922020 and 52090034), and the Fundamental Research Funds for the Central Universities (Nos. BHYC1707B and XK1802-2).

REFERENCES

1 Iqbal, A.; Sambyal, P.; Koo, C. M. 2D MXenes for electromagnetic shielding: a review. *Adv. Funct. Mater.* **2020**, *30*, 2000883.
2 Liang, C.; Gu, Z.; Zhang, Y.; Ma, Z.; Qiu, H.; Gu, J. Structural design strategies of polymer matrix composites for electromagnetic interference shielding: a review. *Nano-Micro Lett.* **2021**, *13*, 181.
3 Song, P.; Liu, B.; Qiu, H.; Shi, X.; Cao, D.; Gu, J. MXenes for polymer matrix electromagnetic interference shielding composites: a review. *Compos. Commun.* **2021**, *24*, 100653.
4 Liu, J.; Zhang, H. B.; Sun, R.; Liu, Y.; Liu, Z.; Zhou, A.; Yu, Z. Z. Hydrophobic, flexible, and lightweight mxene foams for high-performance electromagnetic-interference shielding. *Adv. Mater.* **2017**, *29*, 1702367.
5 Wu, X. Y. Zhang, H. B. Study on structure design and electromagnetic shielding properties of polymer

nanocomposites. *Acta Polymerica Sinica* (in Chinese) **2020**, *51*, 573–585.
6 Sun, R.; Zhang, H.-B.; Liu, J.; Xie, X.; Yang, R.; Li, Y.; Hong, S.; Yu, Z. Z. Highly conductive transition metal carbide/carbonitride (MXene)@polystyrene nanocomposites fabricated by electrostatic assembly for highly efficient electromagnetic interference shielding. *Adv. Funct. Mater.* **2017**, *27*, 1702807.
7 Ma, T. B.; Ma, H.; Ruan, K. P.; Shi, X. T.; Qiu, H.; Gao, S. Y.; Gu, J. W. Thermally conductive poly(lactic acid) composites with superior electromagnetic shielding performances *via* 3D printing technology. *Chinese J. Polym. Sci.* **2022**, *40*, 248–255.
8 Zhang, Q. Y.; Li, H. S.; Guo, B. H.; Guo, Z. X.; Yu, J. Facile preparation of electromagnetic interference shielding materials enabled by constructing interconnected network of multi-walled carbon nanotubes in a miscible polymeric blend. *Chinese J. Polym. Sci.* **2020**, *38*, 593–598.
9 Xu, Y.; Yang, Y.; Yan, D.-X.; Duan, H.; Zhao, G.; Liu, Y. Flexible and conductive polyurethane composites for electromagnetic shielding and printable circuit. *Chem. Eng. J.* **2019**, *360*, 1427–1436.
10 Cao, W. T.; Chen, F. F.; Zhu, Y. J.; Zhang, Y. G.; Jiang, Y. Y.; Ma, M. G.; Chen, F. Binary strengthening and toughening of MXene/cellulose nanofiber composite paper with nacre-inspired structure and superior electromagnetic interference shielding properties. *ACS Nano* **2018**, *12*, 4583–4593.
11 Cao, W. T.; Ma, C.; Tan, S.; Ma, M. G.; Wan, P. B.; Chen, F. Ultrathin and flexible CNTs/MXene/cellulose nanofibrils composite paper for electromagnetic interference shielding. *Nano-Micro Lett.* **2019**, *11*, 72.
12 Shen, B.; Zhai, W.; Zheng, W. Ultrathin flexible graphene film: an excellent thermal conducting material with efficient EMI shielding. *Adv. Funct. Mater.* **2014**, *24*, 4542–4548.
13 Wen, B.; Cao, M.; Lu, M.; Cao, W.; Shi, H.; Liu, J.; Wang, X.; Jin, H.; Fang, X.; Wang, W.; Yuan, J. Reduced graphene oxides: light-weight and high-efficiency electromagnetic interference shielding at elevated temperatures. *Adv. Mater.* **2014**, *26*, 3484–3489.
14 Ma, H. L.; Zhang, H. B.; Hu, Q. H.; Li, W. J.; Jiang, Z. G.; Yu, Z. Z.; Dasari, A. Functionalization and reduction of graphene oxide with p-phenylene diamine for electrically conductive and thermally stable polystyrene composites. *ACS Appl. Mater. Interfaces* **2012**, *4*, 1948–1953.
15 Zeng, Z.; Chen, M.; Jin, H.; Li, W.; Xue, X.; Zhou, L.; Pei, Y.; Zhang, H.; Zhang, Z. Thin and flexible multi-walled carbon nanotube/waterborne polyurethane composites with high-performance electromagnetic interference shielding. *Carbon* **2016**, *96*, 768–777.
16 Jia, L. C.; Li, M. Z.; Yan, D. X.; Cui, C. H.; Wu, H. Y.; Li, Z. M. A strong and tough polymer-carbon nanotube film for flexible and efficient electromagnetic interference shielding. *J. Mater. Chem. C* **2017**, *5*, 8944–8951.
17 Wang, T.; Yu, W. C.; Zhou, C. G.; Sun, W. J.; Zhang, Y. P.; Jia, L. C.; Gao, J. F.; Dai, K.; Yan, D. X.; Li, Z. M. Self-healing and flexible carbon nanotube/polyurethane composite for efficient electromagnetic interference shielding. *Compos. B* **2020**, *193*, 108015.
18 Luo, J. Q.; Zhao, S.; Zhang, H. B.; Deng, Z.; Li, L.; Yu, Z. Z. Flexible, stretchable and electrically conductive MXene/natural rubber nanocomposite films for efficient electromagnetic interference shielding. *Compos. Sci. Technol.* **2019**, *182*, 107754.
19 Jin, X.; Wang, J.; Dai, L.; Liu, X.; Li, L.; Yang, Y.; Cao, Y.; Wang, W.; Wu, H.; Guo, S. Flame-retardant poly(vinyl alcohol)/MXene multilayered films with outstanding electromagnetic interference shielding and thermal conductive performances. *Chem. Eng. J.* **2020**, *380*, 122475.
20 Wang, L.; Chen, L.; Song, P.; Liang, C.; Lu, Y.; Qiu, H.; Zhang, Y.; Kong, J.; Gu, J. Fabrication on the annealed $Ti_3C_2T_x$ MXene/epoxy nanocomposites for electromagnetic interference shielding application. *Compos. B* **2019**, *171*, 111–118.
21 Rajavel, K.; Luo, S.; Wan, Y.; Yu, X.; Hu, Y.; Zhu, P.; Sun, R.; Wong, C. 2D $Ti_3C_2T_x$ MXene/polyvinylidene fluoride (PVDF) nanocomposites for attenuation of electromagnetic radiation with excellent heat dissipation. *Compos. A* **2020**, *129*, 105693.
22 Ma, Z.; Kang, S.; Ma, J.; Shao, L.; Zhang, Y.; Liu, C.; Wei, A.; Xiang, X.; Wei, L.; Gu, J. Ultraflexible and mechanically strong double-layered aramid nanofiber-$Ti_3C_2T_x$ MXene/silver nanowire nanocomposite papers for high-performance electromagnetic interference shielding. *ACS Nano* **2020**, *14*, 8368–8382.
23 Zhou, B.; Zhang, Z.; Li, Y.; Han, G.; Feng, Y.; Wang, B.; Zhang, D.; Ma, J.; Liu, C. Flexible, robust, and multifunctional electromagnetic interference shielding film with alternating cellulose nanofiber and MXene layers. *ACS Appl. Mater. Interfaces* **2020**, *12*, 4895–4905.
24 Yan, D; Zhang, H. B.; Jia, Y.; Hu, J.; Qi, X. Y.; Zhang, Z.; Yu, Z. Z. Improved electrical conductivity of polyamide 12/graphene nanocomposites with maleated polyethylene-octene rubber prepared by melt compounding. *ACS Appl. Mater. Interfaces* **2012**, *4*, 4740–4745.
25 Wu, H. Y.; Jia, L. C.; Yan, D. X.; Gao, J. F.; Zhang, X. P.; Ren, P. G.; Li, Z. M. Simultaneously improved electromagnetic interference shielding and mechanical performance of segregated carbon nanotube/polypropylene composite *via* solid phase molding. *Compos. Sci. Technol.* **2018**, *156*, 87–94.
26 Huang, Y.; Ellingford, C.; Bowen, C.; McNally, T.; Wu, D.; Wan, C. Tailoring the electrical and thermal conductivity of multi-component and multi-phase polymer composites. *Int. Mater. Rev.* **2019**, *65*, 129–163.
27 Jiang, Y.; Sun, R.; Zhang, H. B.; Min, P.; Yang, D.; Yu, Z. Z. Graphene-coated ZnO tetrapod whiskers for thermally and electrically conductive epoxy composites. *Compos. A* **2017**, *94*, 104–112.
28 Yuan, F. Y.; Zhang, H. B.; Li, X.; Li, X. Z.; Yu, Z. Z. Synergistic effect of boron nitride flakes and tetrapod-shaped ZnO whiskers on the thermal conductivity of electrically insulating phenol formaldehyde composites. *Compos. A* **2013**, *53*, 137–144.
29 Lipton, J.; Weng, G. M.; Alhabeb, M.; Maleski, K.; Antonio, F.; Kong, J.; Gogotsi, Y.; Taylor, A. D. Mechanically strong and electrically conductive multilayer MXene nanocomposites. *Nanoscale* **2019**, *11*, 20295–20300.
30 Yu, B.; Zhao, Z.; Fu, S.; Meng, L.; Liu, Y.; Chen, F.; Wang, K.; Fu, Q. Fabrication of PLA/CNC/CNT conductive composites for high electromagnetic interference shielding based on Pickering emulsions method. *Compos. A* **2019**, *125*, 105558.
31 Wu, X.; Lu, C.; Zhang, X.; Zhou, Z. Conductive natural rubber/carbon black nanocomposites via cellulose nanowhisker templated assembly: Tailored hierarchical structure leading to synergistic property enhancements. *J. Mater. Chem. A* **2015**, *3*, 13317–13323.
32 Liu, Z.; Zhang, Y.; Zhang, H. B.; Dai, Y.; Liu, J.; Li, X.; Yu, Z. Z. Electrically conductive aluminum ion-reinforced mxene films for efficient electromagnetic interference shielding. *J. Mater. Chem. C* **2020**, *8*, 1673–1678.
33 Jia, L. C.; Zhou, C. G.; Sun, W.-J.; Xu, L.; Yan, D. X.; Li, Z. M. Water-based conductive ink for highly efficient electromagnetic interference shielding coating. *Chem. Eng. J.* **2020**, *384*, 123368.
34 Xu, Y.; Yang, Y.; Yan, D.-X.; Duan, H.; Zhao, G.; Liu, Y. Gradient structure design of flexible waterborne polyurethane conductive films for ultraefficient electromagnetic shielding with low reflection characteristic. *ACS Appl. Mater. Interfaces* **2018**, *10*, 19143–19152.

https://doi.org/10.1007/s10118-022-2813-2

35 Zhou, B.; Su, M.; Yang, D.; Han, G.; Feng, Y.; Wang, B.; Ma, J.; Ma, J.; Liu, C.; Shen, C. Flexible MXene/silver nanowire-based transparent conductive film with electromagnetic interference shielding and electro-photo-thermal performance. *ACS Appl. Mater. Interfaces* **2020**, *12*, 40859–40869.

36 Luo, J.; Huo, L.; Wang, L.; Huang, X.; Li, J.; Guo, Z.; Gao, Q.; Hu, M.; Xue, H.; Gao, J. Superhydrophobic and multi-responsive fabric composite with excellent electro-photo-thermal effect and electromagnetic interference shielding performance. *Chem. Eng. J.* **2020**, *391*, 123537.

37 Deng, Z.; Tang, P.; Wu, X.; Zhang, H. B.; Yu, Z. Z. Superelastic, ultralight, and conductive $Ti_3C_2T_x$ MXene/acidified carbon nanotube anisotropic aerogels for electromagnetic interference shielding. *ACS Appl. Mater. Interfaces* **2021**, *13*, 20539–20547.

38 Wu, X.; Tu, T.; Dai, Y.; Tang, P.; Zhang, Y.; Deng, Z.; Li, L.; Zhang, H. B.; Yu, Z. Z. Direct ink writing of highly conductive MXene frames for tunable electromagnetic interference shielding and electromagnetic wave-induced thermochromism. *Nano-Micro Lett.* **2021**, *13*, 148.

39 Wang, Q. W.; Zhang, H. B.; Liu, J.; Zhao, S.; Xie, X.; Liu, L.; Yang, R.; Koratkar, N.; Yu, Z. Z. Multifunctional and water-resistant MXene-decorated polyester textiles with outstanding electromagnetic interference shielding and Joule heating performances. *Adv. Funct. Mater.* **2019**, *29*, 1806819.

40 Wu, X.; Han, B.; Zhang, H.-B.; Xie, X.; Tu, T.; Zhang, Y.; Dai, Y.; Yang, R.; Yu, Z. Z. Compressible, durable and conductive polydimethylsiloxane-coated MXene foams for high-performance electromagnetic interference shielding. *Chem. Eng. J.* **2020**, *381*, 122622.

41 Han, M.; Yin, X.; Kong, L.; Li, M.; Duan, W.; Zhang, L.; Cheng, L. Graphene-wrapped ZnO hollow spheres with enhanced electromagnetic wave absorption properties. *J. Mater. Chem. A* **2014**, *2*, 16403–16409.

42 Park, T. H.; Yu, S.; Koo, M.; Kim, H.; Kim, E. H.; Park, J. E.; Ok, B.; Kim, B.; Noh, S. H.; Park, C.; Kim, E.; Koo, C. M.; Park, C. Shape-adaptable 2D titanium carbide (MXene) heater. *ACS Nano* **2019**, *13*, 6835–6844.

43 Zhao, S.; Li, L.; Zhang, H. B.; Qian, B.; Luo, J. Q.; Deng, Z.; Shi, S.; Russell, T. P.; Yu, Z. Z. Janus MXene nanosheets for macroscopic assemblies. *Mater. Chem. Front.* **2020**, *4*, 910–917.

44 Pujari, S. P.; Scheres, L.; Marcelis, A. T.; Zuilhof, H. Covalent surface modification of oxide surfaces. *Angew. Chem. Int. Ed.* **2014**, *53*, 6322–6356.

45 He, H.; Fu, Y.; Zang, W.; Wang, Q.; Xing, L.; Zhang, Y.; Xue, X. A flexible self-powered T-ZnO/PVDF/fabric electronic-skin with multi-functions of tactile-perception, atmosphere-detection and self-clean. *Nano Energy* **2017**, *31*, 37–48.

46 Lu, Y.; Wang, W. Y.; Xue, F.; Yang, J. H.; Qi, X. D.; Zhou, Z. W.; Wang, Y. Bio-inspired polydopamine-assisted graphene oxide coating on tetra-pod zinc oxide whisker for dielectric composites. *Chem. Eng. J.* **2018**, *345*, 353–363.

47 Scaffaro, R.; Botta, L.; Lo Re, G.; Bertani, R.; Milani, R.; Sassi, A. Surface modification of poly(ethylene-*co*-acrylic acid) with amino-functionalized silica nanoparticles. *J. Mater. Chem.* **2011**, *21*, 3849–3857.

48 Zhang, H. B.; Zheng, W. G.; Yan, Q.; Yang, Y.; Wang, J. W.; Lu, Z. H.; Ji, G. Y.; Yu, Z. Z. Electrically conductive polyethylene terephthalate/graphene nanocomposites prepared by melt compounding. *Polymer* **2010**, *51*, 1191–1196.

49 Thongruang, W.; Balik, C. M.; Spontak, R. J. Volume-exclusion effects in polyethylene blends filled with carbon black, graphite, or carbon fiber. *J. Polym. Sci., Part B: Polym. Phys.* **2002**, *40*, 1013–1025.

50 Schutt, F.; Signetti, S.; Kruger, H.; Roder, S.; Smazna, D.; Kaps, S.; Gorb, S. N.; Mishra, Y. K.; Pugno, N. M.; Adelung, R. Hierarchical self-entangled carbon nanotube tube networks. *Nat. Commun.* **2017**, *8*, 1215.

51 Qi, X. Y.; Yan, D.; Jiang, Z.; Cao, Y. K.; Yu, Z. Z.; Yavari, F.; Koratkar, N. Enhanced electrical conductivity in polystyrene nanocomposites at ultra-low graphene content. *ACS Appl. Mater. Interfaces* **2011**, *3*, 3130–3133.

52 Bao, H.-D.; Guo, Z.-X.; Yu, J. Effect of electrically inert particulate filler on electrical resistivity of polymer/multi-walled carbon nanotube composites. *Polymer* **2008**, *49*, 3826–3831.

53 Zhang, Y. P.; Zhou, C. G.; Sun, W.-J.; Wang, T.; Jia, L. C.; Yan, D. X.; Li, Z. M. Injection molding of segregated carbon nanotube/polypropylene composite with enhanced electromagnetic interference shielding and mechanical performance. *Compos. Sci. Technol.* **2020**, *197*, 108253.

54 Zhao, S.; Zhang, H. B.; Luo, J. Q.; Wang, Q. W.; Xu, B.; Hong, S.; Yu, Z. Z. Highly electrically conductive three-dimensional $Ti_3C_2T_x$ MXene/reduced graphene oxide hybrid aerogels with excellent electromagnetic interference shielding performances. *ACS Nano* **2018**, *12*, 11193–11202.

55 Shahzad, F.; Alhabeb, M.; Hatter, C. B.; Anasori, B.; Hong, S. M.; Koo, C. M.; Gogotsi, Y. Electromagnetic interference shielding with 2D transition metal carbides (MXenes). *Science* **2016**, *353*, 1137–1140.

56 Chen, Y.; Zhang, H. B.; Yang, Y.; Wang, M.; Cao, A.; Yu, Z. Z. High-performance epoxy nanocomposites reinforced with three-dimensional carbon nanotube sponge for electromagnetic interference shielding. *Adv. Funct. Mater.* **2016**, *26*, 447–455.

57 Hsiao, S. T.; Ma, C. C. M.; Liao, W. H.; Wang, Y. S.; Li, S. M.; Huang, Y. C.; Yang, R. B.; Liang, W. F. Lightweight and flexible reduced graphene oxide/water-borne polyurethane composites with high electrical conductivity and excellent electromagnetic interference shielding performance. *ACS Appl. Mater. Interfaces* **2014**, *6*, 10667–10678.

58 Li, P.; Du, D.; Guo, L.; Guo, Y.; Ouyang, J. Stretchable and conductive polymer films for high-performance electromagnetic interference shielding. *J. Mater. Chem. C* **2016**, *4*, 6525.

59 Liu, J.; Liu, Z.; Zhang, H. B.; Chen, W.; Zhao, Z.; Wang, Q. W.; Yu, Z. Z. Ultrastrong and highly conductive mxene-based films for high-performance electromagnetic interference shielding. *Adv. Electron. Mater.* **2020**, *6*, 1901094.

60 Liang, C.; Ruan, K.; Zhang, Y.; Gu, J. Multifunctional flexible electromagnetic interference shielding silver nanowires/cellulose films with excellent thermal management and Joule heating performances. *ACS Appl. Mater. Interfaces* **2020**, *12*, 18023–18031.

61 Ma, Z.; Kang, S.; Ma, J.; Shao, L.; Wei, A.; Liang, C.; Gu, J.; Yang, B.; Dong, D.; Wei, L.; Ji, Z. High-performance and rapid-response electrical heaters based on ultraflexible, heat-resistant, and mechanically strong aramid nanofiber/Ag nanowire nanocomposite papers. *ACS Nano* **2019**, *13*, 7578–7590.

62 Hu, P.; Lyu, J.; Fu, C.; Gong, W. B.; Liao, J.; Lu, W.; Chen, Y.; Zhang, X. Multifunctional aramid nanofiber/carbon nanotube hybrid aerogel films. *ACS Nano* **2020**, *14*, 688–697.

63 Liu, X.; Jin, X.; Li, L.; Wang, J.; Yang, Y.; Cao, Y.; Wang, W. Air-permeable, multifunctional, dual-energy-driven MXene-decorated polymeric textile-based wearable heaters with exceptional electrothermal and photothermal conversion performance. *J. Mater. Chem. A* **2020**, *8*, 12526–12537.

64 Fan, X.; Ding, Y.; Liu, Y.; Liang, J.; Chen, Y. Plasmonic $Ti_3C_2T_x$ MXene enables highly efficient photothermal conversion for healable and transparent wearable device. *ACS Nano* **2019**, *13*, 8124–8134.

65 Xu, D.; Li, Z.; Li, L.; Wang, J. Insights into the photothermal conversion of 2D MXene nanomaterials: synthesis, mechanism, and applications. *Adv. Funct. Mater.* **2020**, *30*, 2000712.

66 Li, R.; Zhang, L.; Shi, L.; Wang, P. MXene Ti_3C_2: an Effective 2D light-to-heat conversion material. *ACS Nano* **2017**, *11*, 3752–3759.

https://doi.org/10.1007/s10118-022-2813-2